Electronic Supplementary Material (ESI) for ChemComm.

# Tunable transition metal complexes as hole transport materials for stable perovskite solar cells

Liangyou Lin,[a,b] Camilla Lian,[a] Timothy W. Jones,[a] Robert D. Bennett,[c] Blago Mihaylov,[a] Terry Chien-Jen Yang,[a] Jacob Tse-Wei Wang,[a,d] Bo Chi,[e] Noel W. Duffy,[c] Jinhua Li,[b] Xianbao Wang,[b] Henry J. Snaith,[d] and Gregory J. Wilson[a]

[a]CSIRO Energy Centre, Mayfield West NSW 2304 Australia.

[b]Hubei Collaborative Innovation Centre for Advanced Organic Chemical Materials, Key Laboratory for the Green Preparation and Application of Functional Materials, Ministry of Education, Hubei Key Laboratory of Polymer Materials, School of Materials Science and Engineering, Hubei University, Wuhan, 430062, China

[c]CSIRO Clayton, Energy Laboratories, Clayton South Vic. 3169, Australia.

[d]Department of Physics, Condensed Matter Physics, Clarendon Laboratories, University of Oxford, OX1 3EU, UK

[e]School of Materials Science and Engineering Huazhong University of Science & Technology, Wuhan 430074, China

## Experimental

*Materials:*

In the preparation of redox complexes 2,2’-bipyridine (bpy; Sigma-Aldrich) was used, in addition to substituted bpy-ligands: 4,4’-dimethoxy-bpy (DMObpy; Sigma-Aldrich), 4,4’-diamino-bpy (DAbpy; Carbosynth Ltd) and 4,4’-di-*tert*-butyl-bpy (DTBbpy; Sigma-Aldrich). Iron(Ⅱ) trifluoromethanesulfonate ($CF_3SO_3^-$; triflate) (Sigma Aldrich, >85%). Silver triflate was used as an oxidising agent to access the corresponding Fe(Ⅲ) complex. The coordination compounds were prepared through modified synthetic procedures as previously reported by Kashifand and co-workers.[1]

Perovskite solution precursor reagents were as follows: methylammonium bromide ($CH_3NH_3Br$, MABr, Greatcell Solar Materials), formamidinium iodide ($(NH_2)_2CHI$ FAI, Greatcell Solar Materials), cesium iodide (CsI, 99.995% Sigma-Aldrich), lead iodide ($PbI_2$, TCI), lead bromide ($PbBr_2$, TCI).

Charge selective transport layers were prepared from $SnCl_2{\cdot}2H_2O$ (Sigma-Aldrich), $SnO_2$ colloid, (Alfa Aesar), 2,2',7,7'-Tetrakis[*N*,*N*-di-(4-methoxyphenyl)amino]-9,9'-spirobifluorene (Spiro-OMeTAD, 99.9%, Lumtec), lithium bistrifluoromethanesulfonimide (LiTFSI, Sigma-Aldrich) and tert-butyl pyridine (tBP, Sigma Aldrich).

Unless otherwise stated, all other reagents and solvents were supplied from Sigma-Aldrich and used as received. All solvents were anhydrous, where available, and used without any further purification.

*Hole Transport Materials:*

*Preparation of Complex Type I: [Fe(pyridyl)$_3$](CF$_3$SO$_3$)$_2$*

$CH_3CN$ (<20 mL) was added to a solid mixture of pyridyl ligand (150-250 mg) and $Fe(CF_3SO_3)_2$ (200 mg). The mixture was stirred for 4 h at 60 °C after which the reaction mixture was cooled and allowed to stand. After cooling to ambient temperature, the solution was filtered through a disposable 0.2 µm PTFE syringe filter and layered with diethyl ether (<100 mL). Solvent diffusion over 2 days allowed micro-crystals of [Fe(pyridyl)$_3$]($CF_3SO_3$)$_2$ to form that were further washed with diethyl ether (3 x 20 mL) and air dried.

*Preparation of Complex Type II: Synthesis of [Fe(pyridyl)$_3$](CF$_3$SO$_3$)$_3$*

$CH_3CN$ (<20 mL) was added to a mixture of [Fe(pyridyl)$_3$]($CF_3SO_3$)$_2$ (100-150 mg) and Ag($CF_3SO_3$) (30-50 mg). The mixture was stirred for 0.5 h at RT after which it had turned a darker colour. The solution was filtered through a disposable PTFE filter and layered with diethyl ether (<100 mL). Solvent diffusion over 2 days allowed crystals of [Fe(pyridyl)$_3$]($CF_3SO_3$)$_3$ to form that were further washed with $Et_2O$ (3 x 20 mL) and dried.

*Device fabrication*:

*Substrate preparation*:

Glass substrates label patterning with a 10.6 µm laser (60 W, Universal Laser Systems) to the rear-side of fluorine-doped tin-oxide (FTO) transparent conducting oxide glass (8 $\Omega\ \square^{-1}$; 2.2 mm substrate thickness, Pilkington) and a cell isolation pattern to the FTO side achieved using a 1.06 µm laser (40 W, Universal Laser Systems).The patterned substrates were rinsed thoroughly in water, then brushed lightly with a solution of 2% v/v% Hellmanex in Milli-Q water (>18.2 MΩ cm) and then sequentially rinsed in Milli-Q water then isopropanol (IPA).

*Compact layer deposition*:

For the bottom $SnO_2$ layer, 0.1M $SnCl_2{\cdot}2H_2O$ precursor solution in absolute ethanol was stirred in ambient conditions (T~22°C, RH~22%) for 2h before spin-coating onto FTO/glass substrates at 4000 rpm for 30 s, followed by annealing at 150 °C for 30 min then 180°C for 60 min. After cooling down to room temperature, $SnO_2$ colloid precursor solution (diluted by Milli-Q $H_2O$, v:v = 1:6) was spin-coated onto $SnO_2$/FTO/glass substrates at 4000 rpm for 30 s, and then annealed at 150°C for 30 min.

*Mixed-cation lead mixed-halide perovskite deposition*:

The perovskite films were deposited from a precursor solution containing formamidinium iodide FAI (1.1M), lead iodide $PbI_2$ (1.2 M), methylammonium bromide MABr (0.2 M) and lead bromide $PbBr_2$ (0.2 M) in a mixture of anhydrous dimethylformamide: dimethylsulfoxide 4:1 (v:v). Then cesium iodide CsI, pre-dissolved in DMSO as a 1.5 M stock solution, was added to the mixed perovskite precursor to achieve the desired triple cation perovskite precursor solution. This solution was then stirred for 2h at room temperature and filtered (0.22 µm PTFE filter) before use. The perovskite solution was spin-coated using a two-step program at 2000 rpm and 4000 rpm for 10 s and 20 s with 200 rpm/s and 1000 rpm/s acceleration, respectively. During the second step, 300 µL of chlorobenzene was fully pipetted onto the spinning substrate 1 s prior to the end of the program. The substrates were then annealed at 100 °C for 30 min in a nitrogen-filled glove box.

*Deposition of Fe-complex layer as the hole transport material (HTM)*:

A solution of 25 mM iron redox couple solution in anhydrous nitromethane was made under a nitrogen atmosphere. The deposited perovskite films were cooled down and blown with $N_2$ to remove potential dust particles before placed in the spin-coater. 50 µL of the Fe-complex solution was then dynamically spin-coated at 4000 rpm for 20 s.

*Rear electrode contact deposition*:

The common contact area of the substrates was mechanically scribed to remove the perovskite and an Au electrode (80 nm) was evaporated on top of the perovskite with a thermal evaporator run with an internal based pressure at $< 5\times10^{-7}$ Torr (Ångström Engineering).

*Device Characterisation*:

The current–voltage (*I*–*V*) characteristics of the cells were recorded with a digital source meter (Keithley model 2400, USA) in a 4-terminal connection. A 450 W Newport Oriel class AAB xenon lamp was used as the light source for photovoltaic (*J*–*V*) measurements. The solar simulator intensity was confirmed against a Si reference cell (Fraunhofer), checked and recorded before each measurement. Typically, the devices were fabricated with an evaporated contact area of 0.10 $cm^2$ and measured with 0.08 $cm^2$ sized aperture unless stated otherwise. Scan sweep rate was performed at 100 mV $s^{-1}$ and no device preconditioning such as light soaking, or forward voltage bias, was applied before starting the measurement. Electrochemical impedance spectroscopy (EIS) were measured with an Autolab PGSTAT 302N potentiostat/galvanostat fitted with an impedance spectroscopy module. Illumination bias was provided by a white light LED. Film thicknesses were measured with a Dektak 1500 profilometer (Veeco Instruments). Photo-stability measurements were conducted under AM 1.5G continuous illumination at a fixed voltage corresponding to the maximum power point of their *I*–*V* measurement. The temperature was maintained at ca. 25°C by a Peltier controlled temperature stage. These devices were encapsulated in a nitrogen glovebox using a UV-curable encapsulant (LT-U001) and a glass coverslip.

*Thin-Film Characterisation*:

Scanning Electron Microscopy (SEM) analyses were performed using a field emission SEM (Zeiss Auriga FIB-FESEM), operated at an accelerating voltage of 5 kV with an In-Lens secondary electron detector. Time-resolved photoluminescence decays were acquired following previous reports using a time-correlated single photon-counting set-up (Horiba; using a 405 nm pulsed laser source operating at repetition rate of 250 kHz). UV-vis spectra were measured with a Perkin-Elmer Lambda 950 spectrophotometer in air. PESA measurements were conducted on a Riken Keiki AC-2 photoelectron spectrometer.

*Cyclic Voltammetry*：

Cyclic voltammetry was recorded using an Autolab PG302N potentiostat in a three-electrode set up. A Pt disc working electrode (1.6 mm ϕ); a Pt wire coil counter electrode, and an Ag|Ag$^+$ reference electrode housed in a Luggin capillary. The reference electrode electrolyte contained 10 mM $AgNO_3$ + 0.1 M tetrabutylammonium hexafluorophosphate ($TBAPF_6$) supporting electrolyte. 10 mM solutions of Fe complex were prepared in dry acetonitrile (stored under nitrogen) with 0.1 M $TBAPF_6$ supporting electrolyte. The voltammetry was recorded at a sweep rate of 100 mV $s^{-1}$. Finally, potentials were referenced to the ferrocene/ferrocenium couple.

**Results:**

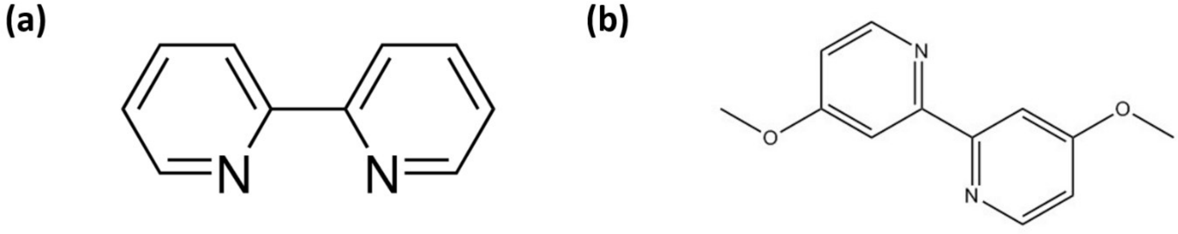

**2,2‘-bipyridine (Bpy)** **4,4'-dimethoxy-2,2'-bipyridine (DMO)**

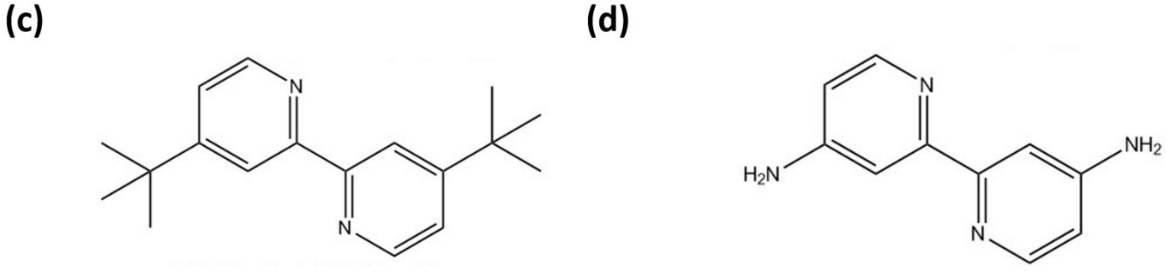

**4,4'-ditertbutyl-2,2'-bipyridine (DTB)** **4,4'-diamino-2,2'-bipyridine (DA)**

Fig. S1 Chemical structures of bipyridyl ligands

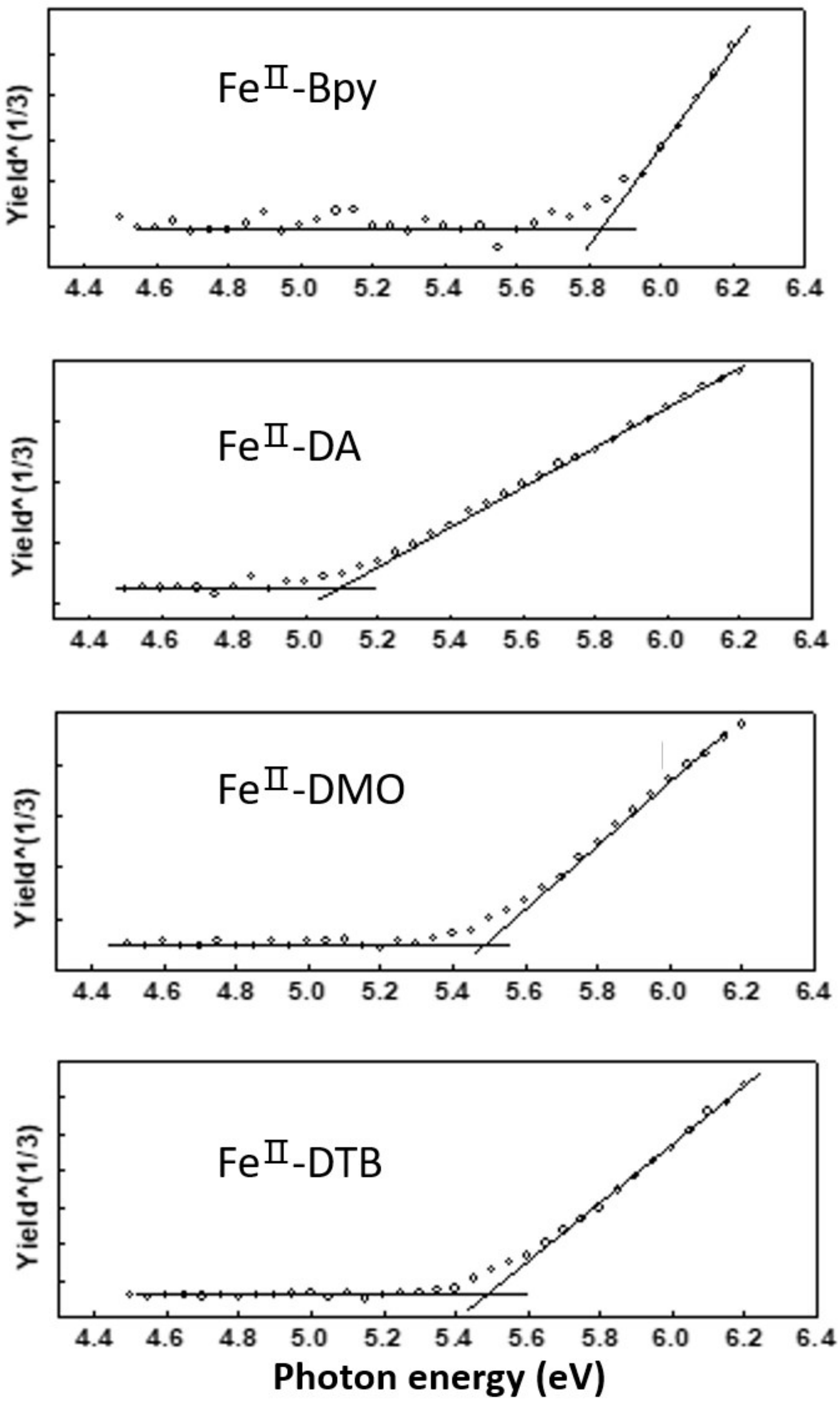

Fig. S2 PESA of each Fe$^{\mathrm{II}}$ complex film made on FTO.

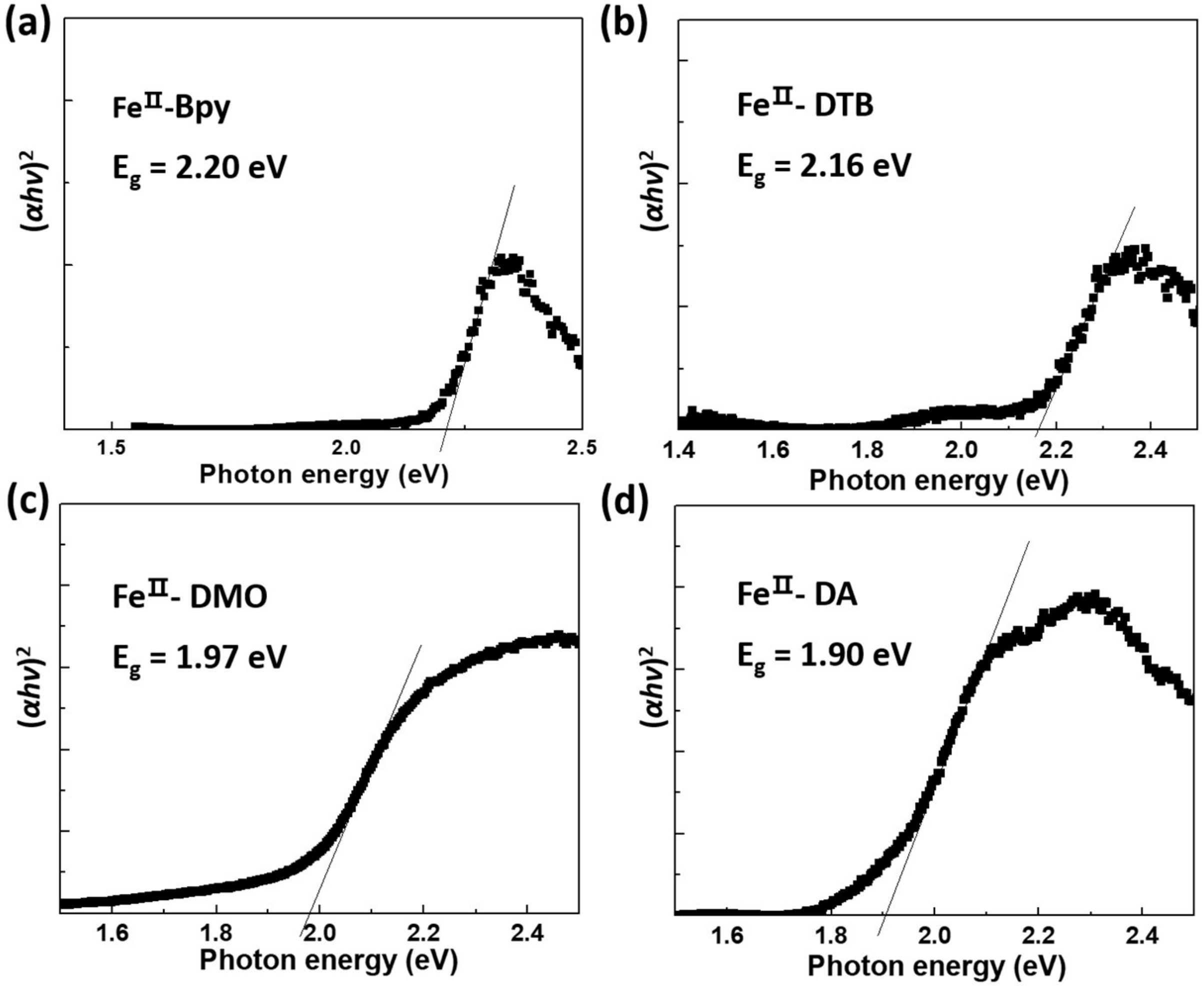

Fig. S3 The optical band-gap derived from Tauc plots of each Fe$^{II}$ complex

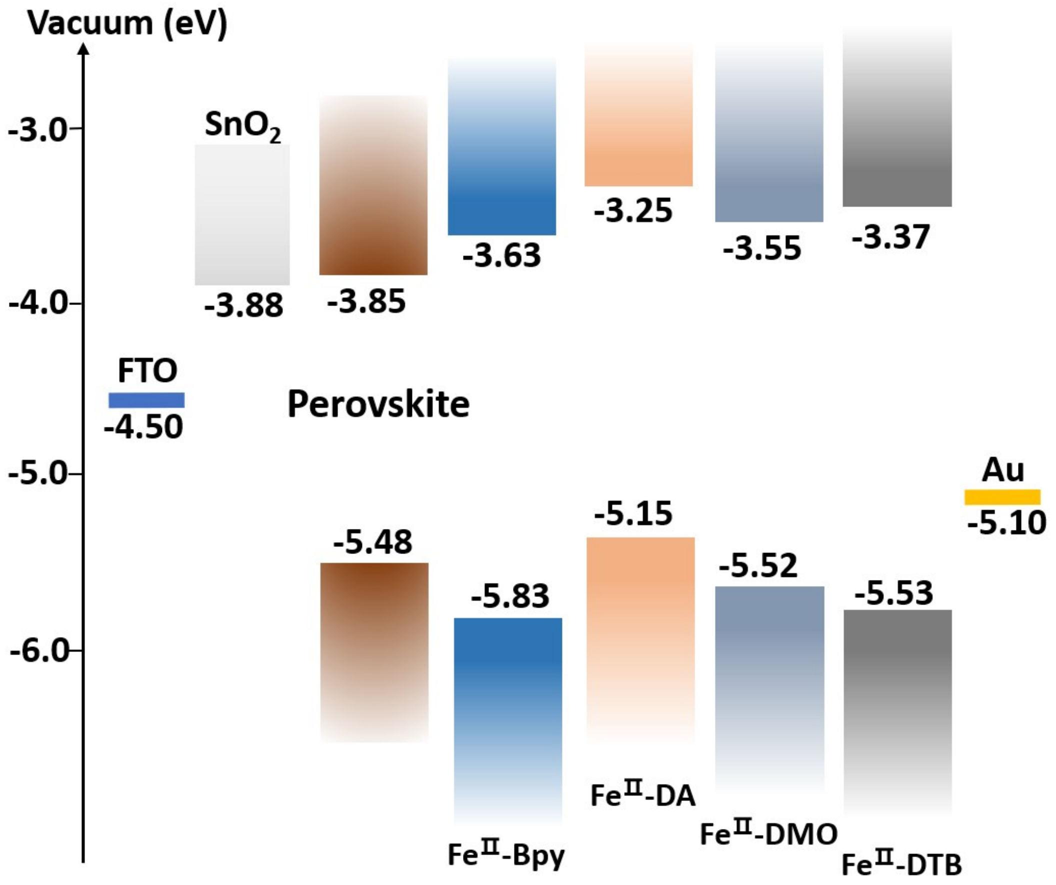

Fig. S4 Energy level alignment diagram

|  | $t_1$(ns) | $A_1$(%) | $t_2$(ns) | $A_2$(%) | Average t (ns) |
|---|---|---|---|---|---|
| Control | 5.8 | 50.8 | 406.7 | 49.2 | 400.9 |
| $\mathrm{Fe}^{\mathrm{II}}$-DTB | 3.0 | 75.8 | 164.8 | 24.2 | 156.2 |
| $\mathrm{Fe}^{\mathrm{II}}$-Bpy | 4.4 | 67.5 | 714.0 | 32.5 | 705.0 |
| $\mathrm{Fe}^{\mathrm{II}}$-DMO | 4.1 | 94.2 | 777.3 | 5.8 | 715.2 |
| $\mathrm{Fe}^{\mathrm{II}}$-DA | 2.0 | 92.1 | 23.9 | 7.9 | 13.0 |

Table S1 Detailed parameters in the fitting results from Figure 1b.

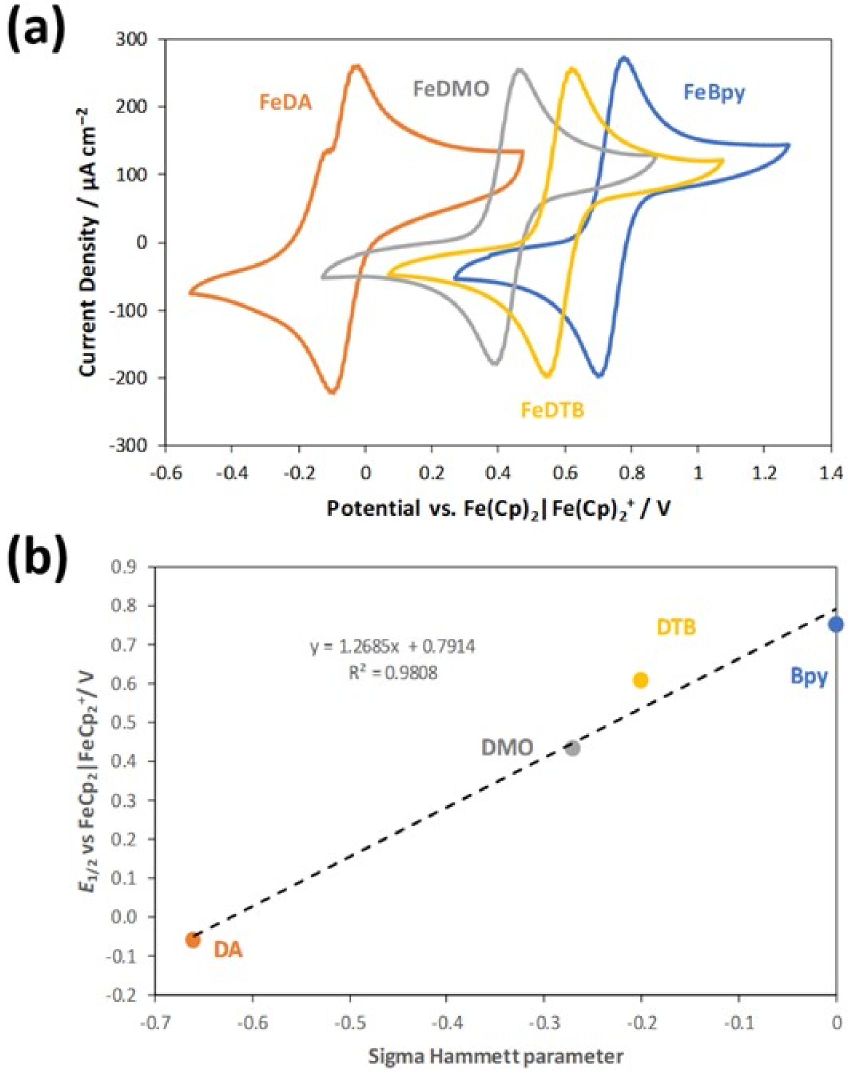

Fig. S5 (a) Cyclic voltammetry of each complex. (b) Corresponding $E_{1/2}$ data.

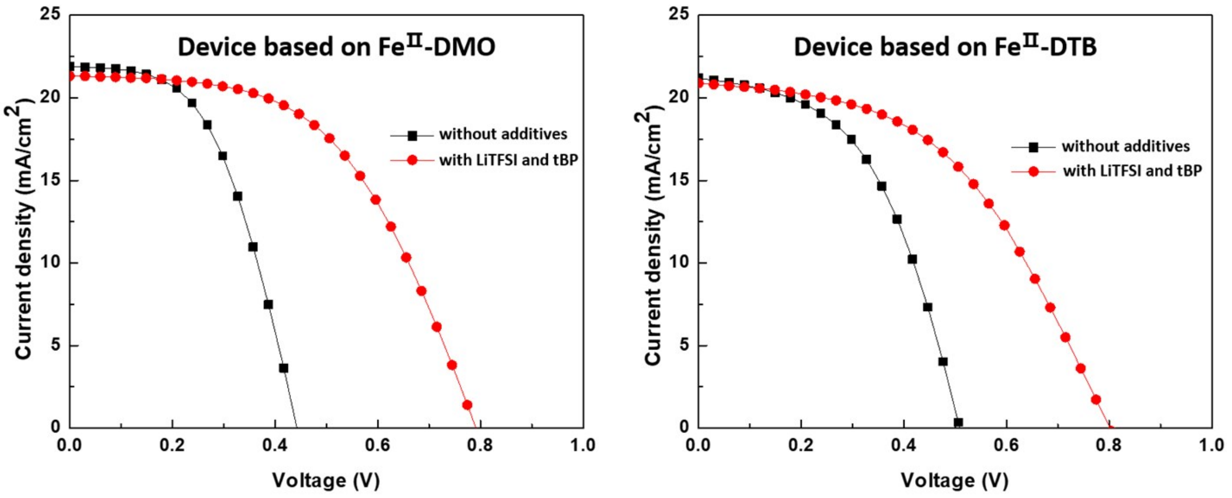

Fig. S6 DTB and DMO with 4-tert-butyl-pyridine and LiTFSI additives boosts performance.

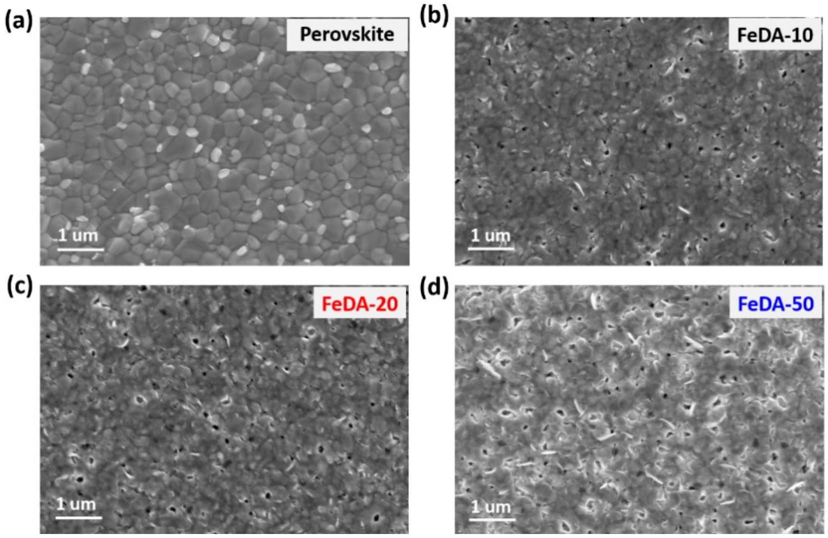

Fig. S7 Top-view SEM images of the bare perovskite film and each Fe-complex film on the bare perovskite films.

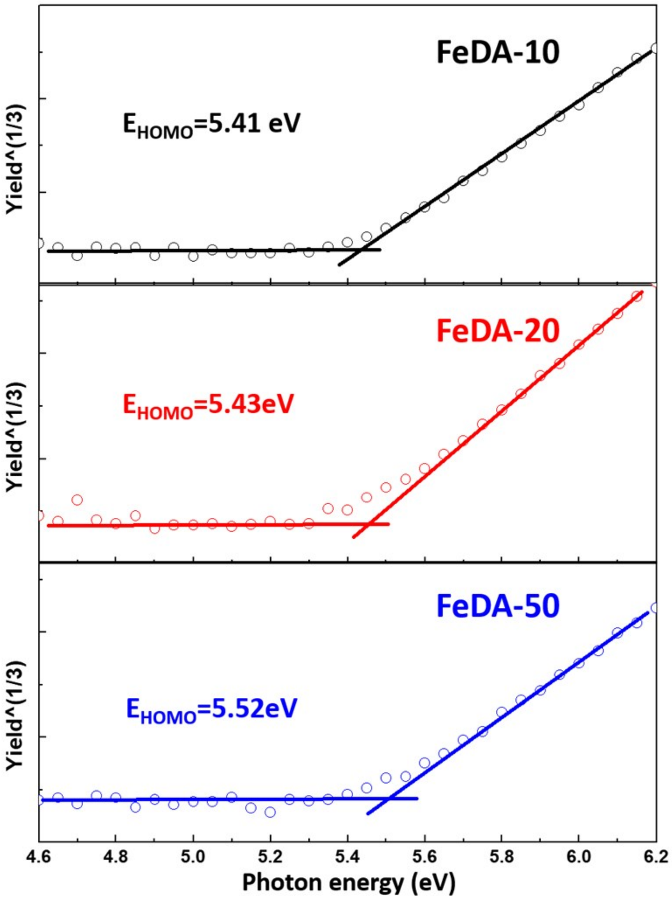

Fig. S8 PESA of FeDA-10, FeDA-20 and FeDA-50 on top of the perovskite film.

| | $t_1$(ns) | $A_1$(%) | $t_2$(ns) | $A_2$(%) | Average t (ns) |
|---|---|---|---|---|---|
| Control | 0.9 | 76.4 | 207.8 | 23.6 | 205.1 |
| FeDA-10 | 0.8 | 89.1 | 24.5 | 10.9 | 19.8 |
| FeDA-20 | 0.8 | 83.4 | 20.6 | 16.6 | 17.5 |
| FeDA-50 | 1.0 | 82.2 | 45.9 | 17.8 | 41.9 |

Table S2 Detailed parameters in the fitting results from Figure 3(b).

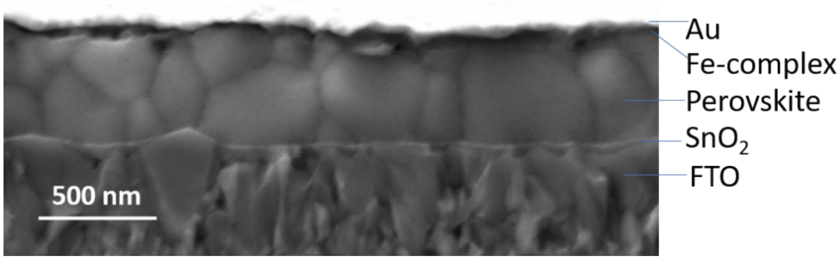

Fig. S9 Cross-sessional SEM images of the device based on FeDA-20 HTL.

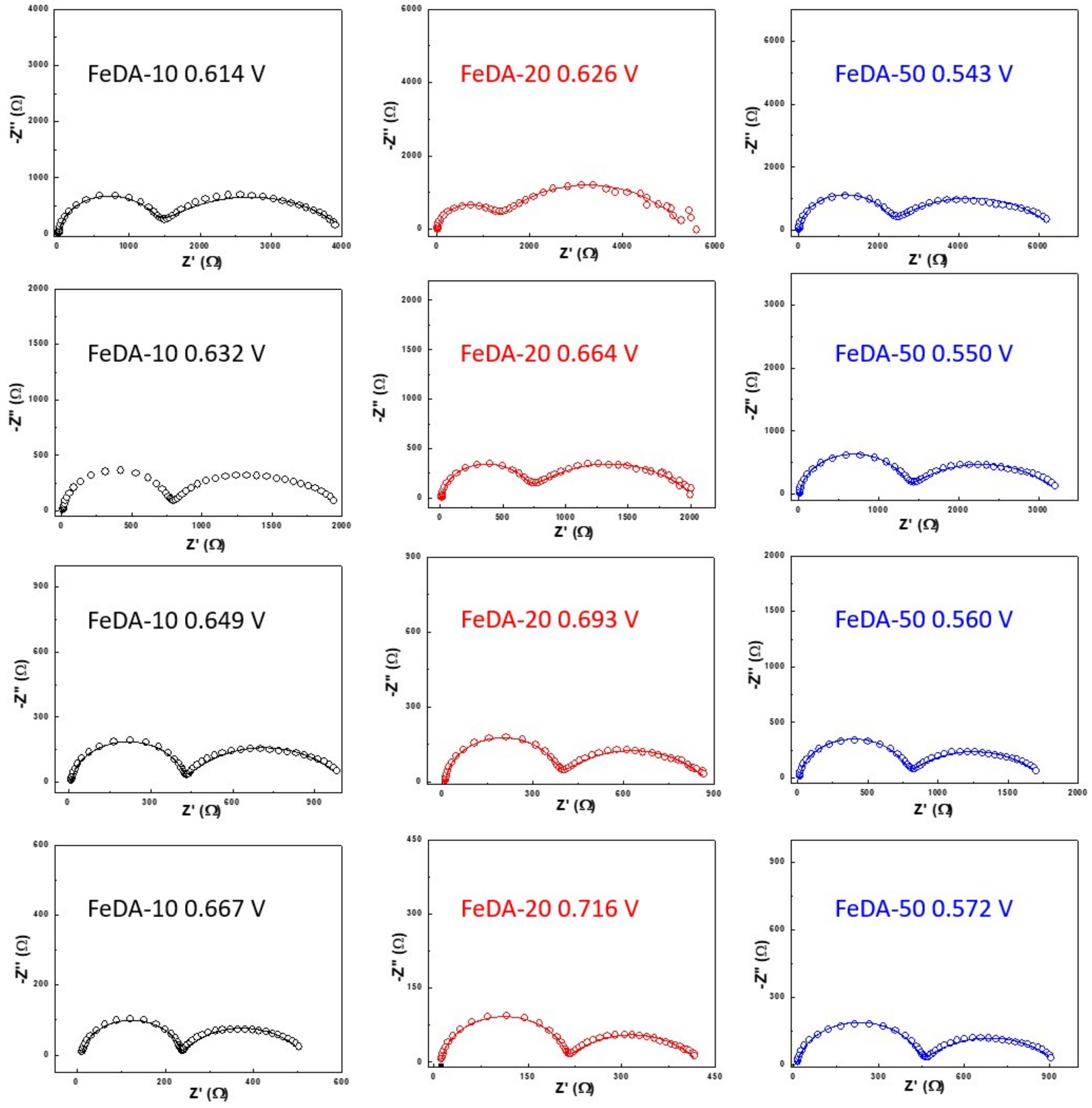

Fig. S10 Nyquist plots and fitting results of devices based on each Fe-complex HTL.

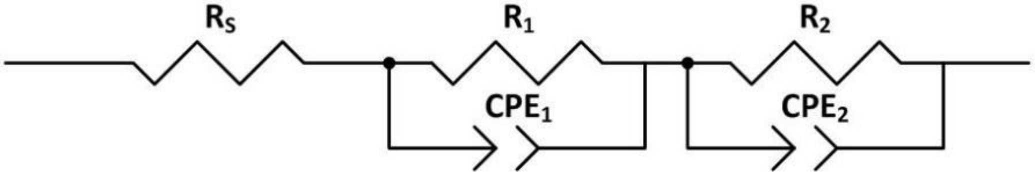

Fig. S11 Equivalent circuit used for fitting in Figure S11.

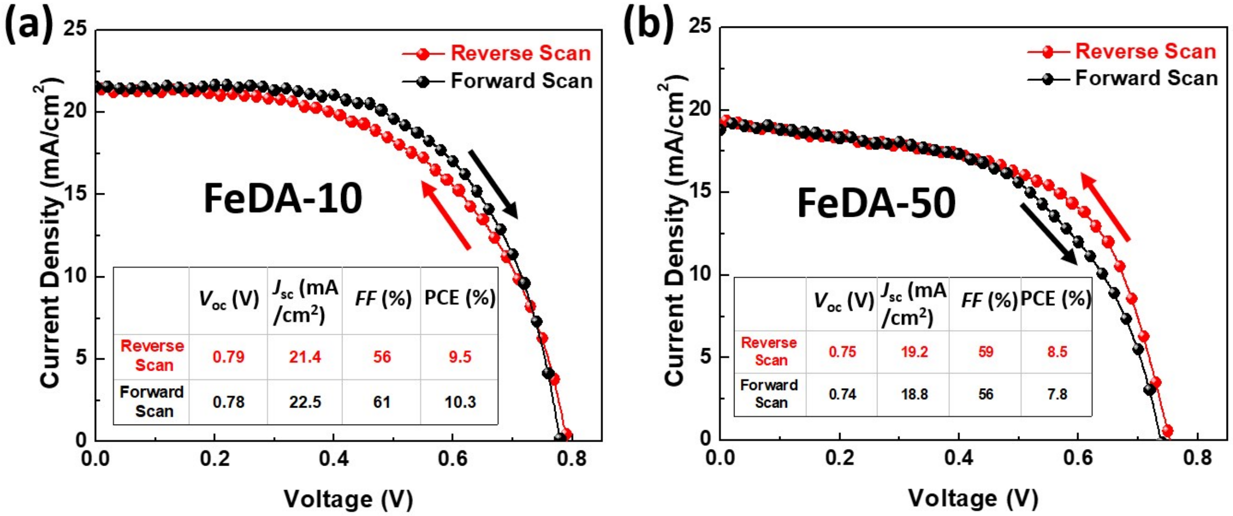

(a) FeDA-10

| | $V_{oc}$ (V) | $J_{sc}$ (mA /cm$^2$) | *FF* (%) | PCE (%) |
|---|---|---|---|---|
| Reverse Scan | 0.79 | 21.4 | 56 | 9.5 |
| Forward Scan | 0.78 | 22.5 | 61 | 10.3 |

(b) FeDA-50

| | $V_{oc}$ (V) | $J_{sc}$ (mA /cm$^2$) | *FF* (%) | PCE (%) |
|---|---|---|---|---|
| Reverse Scan | 0.75 | 19.2 | 59 | 8.5 |
| Forward Scan | 0.74 | 18.8 | 56 | 7.8 |

Fig. S12 *J*-*V* curves of champion devices based on FeDA-10 and FeDA-50.

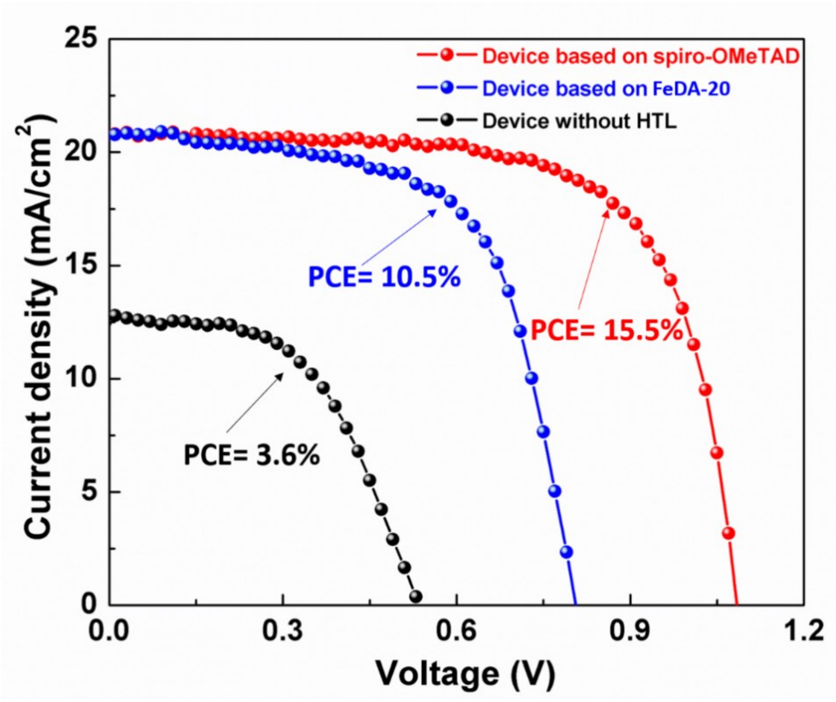

Fig. S13 *J*-*V* curves of the devices based on spiro-OMeTAD, FeDA-20 and without HTL.

References:

1 M. K. Kashif, I. Benesperi, R. A. Milhuisen, S. Meyer, J. Hellerstedt, D. Zee, N. W. Duffy, B. Halstead, M. S. Fuhrer, J. Cashion, Y. B. Cheng, L. Spiccia, A. N. Simonov and U. Bach, *ACS Energy Lett.*, 2017, **2**, 1855–1859.